International Journal of Heat and Fluid Flow 29 (2008) 1679–1687

Contents lists available at ScienceDirect

International Journal of Heat and Fluid Flow

journal homepage: www.elsevier.com/locate/ijhff

PIV measurements of turbulent boundary layer over a rod-roughened wall

Seung-Hyun Lee, Jung Hun Kim, Hyung Jin Sung *

Department of Mechanical Engineering, Korea Advanced Institute of Science and Technology, 373-1, Guseong-dong, Yuseong-gu, Daejeon 305-701, Republic of Korea

ARTICLE INFO

Article history:
Received 15 April 2008
Received in revised form 16 July 2008
Accepted 10 September 2008
Available online 5 November 2008

Keywords:
Particle image velocimetry
Surface roughness
Turbulent boundary layer

ABSTRACT

The effects of surface roughness on a turbulent boundary layer (TBL) were investigated by performing particle image velocimetry (PIV) measurements. The Reynolds number based on the momentum thickness was about $Re_\theta = 1000–1500$. The roughness elements used were periodically arranged two-dimensional spanwise rods, and the ratio of the boundary layer thickness to the roughness height was $k/\delta = 0.025$. Along the streamwise direction, self-preserving forms of the streamwise mean velocity and the turbulent Reynolds stress were obtained. Spatially developing characteristics of the rough wall TBL were examined. Introduction of the roughness elements augmented turbulent stresses in the region of $y < 4–5k_s$, where k_s is an effective sand roughness height. We found that the effective sand roughness height (k_s) is a more appropriate length scale for representing the extent of roughness effect rather than the roughness height (k). By using PIV measurements, the effects of surface roughness on the turbulence structure in the roughness sublayer were examined and compared with previous direct numerical simulation (DNS) results. Iso-contours of the mean velocity and Reynolds stress in the roughness sublayer obtained by PIV were in very good agreement with DNS findings. Vortex structures induced by the rod-roughness and strong sweep events were also examined.

1. Introduction

Turbulent boundary layers (TBLs) are encountered in numerous fluid dynamic engineering applications, and have been examined in many experimental and numerical studies. In real engineering applications involving wall-bounded boundary layer flow (e.g. automobiles, ships, airplanes and heat-exchangers), the roughness of the wall surface is an important design parameter because it influences characteristics such as the transport of heat, mass and momentum. Recently, numerous experimental and numerical studies have added to our understanding of the effects of surface roughness on TBLs.

Previous experimental studies on the effects of surface roughness on TBLs have been well reviewed by Raupach et al. (1991) and Jimenez (2004). These reviews support the wall similarity hypothesis of Townsend (1976), which states that outside the roughness sublayer turbulent motions are independent of the surface roughness and that the interaction between the inner and outer layers is very weak at sufficiently large Reynolds numbers. This hypothesis is further supported by the results obtained by Schultz and Flack (2005, 2007) and Flack et al. (2005, 2007) in experimental studies of TBLs over surfaces with uniform three-dimensional roughness. Specifically, consistent with Townsend's wall similarity hypothesis, they observed that the outer layers of flows past smooth and rough walls were similar in terms of both the mean flow and turbulent statistics.

Results from several experimental studies of TBLs over surfaces with two-dimensional rod-roughness, however, have been contrary to the wall similarity hypothesis. Krogstad et al. (1992) found that the wake strength in a TBL is increased by two-dimensional roughness and that the interaction between the inner and outer layers is non-negligible. In addition, Krogstad and Antonia (1999) and Keirsbulck et al. (2002) observed that turbulent Reynolds stresses in the outer layer of a TBL are significantly affected by two-dimensional rod-roughness. Krogstad and Antonia (1999) compared the effects of rod-roughness and mesh roughness on TBLs and found that TBLs are influenced by the geometry of the surface roughness. These experimental results are not consistent with the notion that the outer layer of a TBL is insensitive to the three-dimensional roughness, and have led to considerable uncertainty regarding the effects of surface roughness on TBLs.

Recently, several numerical studies using direct numerical simulation (DNS) and large eddy simulation (LES) have been conducted on turbulent channel flows with three-dimensional roughness (Lee, 2002; Bhaganagar et al., 2004) or two-dimensional rods (Ashrafian et al., 2004; Leonardi et al., 2003). Krogstad et al. (2005) compared the results of the experimental study of Bakken and Krogstad (2005) on a symmetric channel with a rod-roughness of $k/h = 0.034$ with the results obtained by Ashrafian et al. (2004) in a DNS of a system with the same height of rod-roughness. They observed good agreement between experiment and simulation, with

* Corresponding author. Tel.: +82 42 350 3027; fax: +82 42 350 5027.
E-mail address: hjsung@kaist.ac.kr (H.J. Sung).

0142-727X/$ - see front matter © 2008 Elsevier Inc. All rights reserved.
doi:10.1016/j.ijheatfluidflow.2008.09.006

both showing no significant difference between the characteristics of the outer layer of the system with a smooth wall and that with a rough wall. Note that these results are contrary to the behavior observed by Krogstad and Antonia (1999) in their TBL experiments with a rod-roughened wall, which showed significant roughness effects in the outer layer. Krogstad and Antonia conjectured that the degree to which surface roughness affects the outer layer is influenced by the flow type, for example symmetric channel flow, asymmetric channel flow, boundary layer, and so on.

Despite the fact that most experimental studies have examined the characteristics of TBLs, the majority of numerical studies (LES and DNS) have examined turbulent channel flows. This discrepancy, which can be attributed to the difficulty of simulating TBLs, has led to a scarcity of DNS data for TBLs, making it difficult to validate experiments on rough wall TBLs. Recently, Lee and Sung (2007) performed DNSs of TBLs over smooth and rod-roughened walls, and examined the spatially developing characteristics of the rough wall TBL. They suggested that the introduction of rod-roughness affects the turbulent stresses and vertical turbulent transport not only in the roughness sublayer but also in the outer layer. However, Jimenez (2004) proposed a criterion whereby wall similarity is satisfied if the ratio of the boundary layer thickness to the roughness height (k/δ) is less than or equal to 0.025. The value of this ratio in the system studied by Lee and Sung (2007), $k/\delta = 0.05$, was too large to satisfy the criterion. To perform a DNS of a TBL that satisfies the criterion of Jimenez (2004), a huge domain size and very fine grid spacing must be accommodated, which is computationally very expensive. Note that the DNS study by Ashrafian et al. (2004) of a turbulent channel flow with a two-dimensional rod-roughness similar to that of Lee and Sung (2007) showed excellent similarity between systems with smooth and rough walls even though the rod-roughness was insufficient to satisfy the criterion of Jimenez (2004). This indicates that the wall similarity criterion may not be universal to all flow types, and supports the conjecture that the surface roughness effects on the outer layer depend on the outer boundary condition.

In the present study, we carried out particle image velocimetry (PIV) experiments on a system with two-dimensional rod-roughness ($k/\delta = 0.025$) that satisfies the criterion of Jimenez (2004). The effects of surface roughness on turbulent Reynolds stresses were investigated and the findings were compared with the DNS results of Lee and Sung (2007). The turbulent structures induced by the rod-roughness were investigated using PIV. Although it is difficult to use hot-wire anemometry or laser Doppler velocimetry data to accurately determine the turbulent structure near the roughness sublayer, where the velocity field is highly spatially inhomogeneous, PIV gives more accurate information on the spatial distribution of velocity fields. Recently, PIV has been used in various experimental studies of surface roughness (Islam et al., 2002; Wang et al., 2007; Pokrajac et al., 2007; Volino et al., 2007; Morris et al., 2007; Djenidi et al., 2008). We measured the iso-contours of mean velocity and streamlines in the roughness sublayer, and found that the locations of the vortex core in a cavity, as well as the locations of the local maxima and minima of the wall-normal mean velocity are in very good agreement with those of the DNS. The separated shear layer and vortical structure induced by the two-dimensional rod-roughness were also examined.

2. Experimental apparatus and procedure

Measurements were performed in a recirculating open-water channel driven by a centrifugal pump. A setting chamber, a honeycomb, and a contraction were placed in sequence to ensure flow homogeneity. Fig. 1 shows a schematic of the test section, roughness elements and PIV setup. The dimensions of the test section

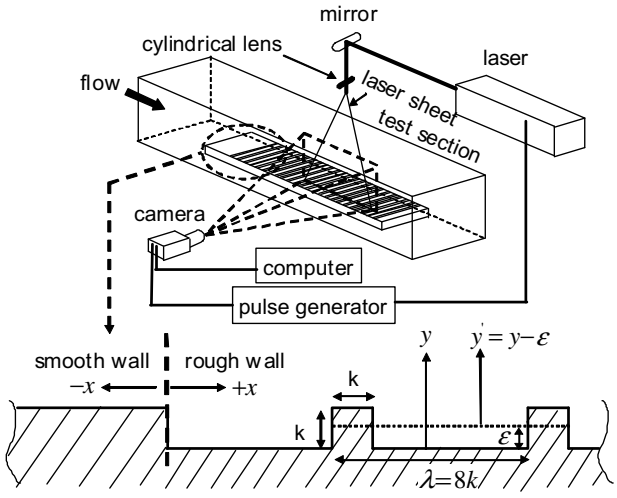

Fig. 1. Schematics of the experimental setup and roughness.

were 250 mm (width) × 275 mm (depth) × 2000 mm (length). The boundary layer was tripped at the leading edge of the flat plate using a combination of a trip wire of diameter 3 mm and a sand grain (CC-80Cw) rough strip. This combination ensured a self-preserving turbulent boundary layer upstream of the first rod-roughness. The free-stream velocity (U_∞) was defined as the streamwise mean velocity near the free surface where mean velocity gradient is negligible. The boundary layer thickness (δ) was defined as the height where the streamwise mean velocity is 99% of the free-stream velocity.

As shown in Fig. 1, two-dimensional spanwise rods with a square cross-section are periodically arranged in the streamwise direction from 700 mm to 1300 mm downstream of the leading edge of the plate. The height of each rod is 2.0 mm and the pitch is $\lambda = 8k$, which corresponds to the k-type roughness. To reduce the effect of the step change at the first roughness element, the surface was lowered by a distance equal to the rod height one period prior to the first rod, as shown in Fig. 1 (Antonia and Luxton, 1971). We defined the streamwise distance (x) from the position where the surface roughness step change occurs from the smooth to the rough wall. The distance is normalized by the boundary layer thickness at the step change region (δ_0), which is 67 mm and 74 mm for the smooth and rough walls, respectively. For the smooth wall, the friction velocity (u_τ) was estimated by the computational Preston method (CPM; Nitche et al., 1983). For the rough wall, the friction velocity was estimated by extrapolating the total shear stress $\tau_w = \mu dU/dy - \rho\overline{uv}$. The position of the virtual origin was estimated using the fitting method of Krogstad et al. (1992). All turbulent statistics data were acquired when the mean velocity and the turbulent Reynolds stresses had reached an equilibrium state. The flow parameters for the smooth and rough walls are summarized in Table 1.

A CCD camera (Kodak ES-1.0, 1024 × 1024 pixel CCD array size) coupled to a PC running image acquisition software was used to acquire images. Hollow glass beads ($\rho = 1.02$ kg/m^3, $d = 8$–12 μm) were used as tracer particles. The flow plane of interest was illuminated with a Nd:YAG laser (Big Sky Laser, Ultra) which was capable

Table 1
Boundary layer parameters

Wall	U_∞ (m/s)	δ (mm)	u_τ (m/s)	Re_θ	k_s^+	k/δ	k_s/δ
Smooth	0.204	66.8	0.0100	1078	–	–	–
Rough	0.205	80.0	0.0133	1491	103	0.025	0.126

of producing 8 ns, 30 mJ pulses at a repetition frequency of 15 Hz. The pulses for the laser and the CCD camera were generated and delayed using a pulse generator (Berkeley Nucleonics, BNC-555). The laser beam was carried by an optical arm and an appropriate combination of cylindrical lenses was employed to produce a collimated light sheet on the center of the channel. At each measurement region, 4800 velocity fields were acquired. The iterative multigrid image processing method (Scarano and Riethmuller, 1999) was used to increase the spatial resolution and correlation based correction (CBC; Hart, 2000) was used to improve the signal-to-noise ratio. For vector post-processing, the local median filter criterion (Westerweel, 1994) was used. The final interrogation window size was 32×32 pixels with a 50% overlap. To measure the entire boundary layer, the field of view of the camera was 97×97 mm for the smooth wall and 105.5×105.5 mm for the rough wall. The resulting spatial resolution of 1.6 mm between measurement points, which corresponds to about 1–2 vectors across the face of the roughness elements, is too coarse to accurately represent turbulence statistics in the roughness sublayer. Therefore, high-resolution PIV measurements were carried out for the rough wall to analyze the turbulent structure in the roughness sublayer, where the field of view of the camera was about 26.3 mm $\times$ 26.3 mm and the final interrogation window size was 16×16 pixels with a 50% overlap. This gave a spatial resolution of 0.21 mm between measurement points, which corresponds to 10 vectors across the face of the roughness element.

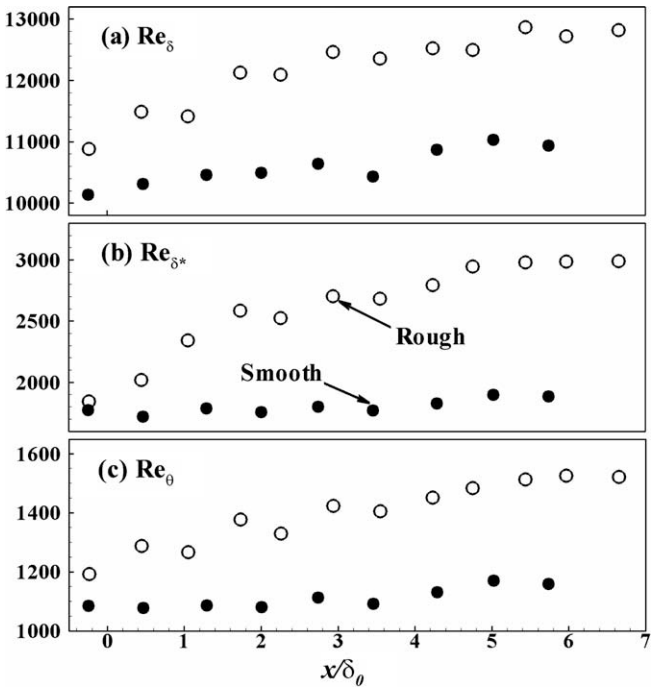

Fig. 2. Variations of the Reynolds numbers, normalized by the boundary layer thickness, displacement thickness and momentum thickness along the downstream over the smooth and rough walls.

3. Results and discussion

Fig. 2 shows the variations of the Reynolds numbers, normalized by the boundary layer thickness, displacement thickness and momentum thickness, with moving downstream over the smooth and rough walls. For each type of normalization, the rate of increase of the Reynolds number with moving downstream is faster for the rough wall than for the smooth wall. In the present study, the step change effect of surface roughness is much smaller than that observed in the DNS of Lee and Sung (2007). This can be attributed to two factors. First, the ratio of the roughness height to the boundary layer thickness at the first rod (k/δ_0) was $k/\delta_0 = 0.027$ in the present experiments (see Fig. 1), but was $k/\delta_0 = 0.125$ in the DNS of Lee and Sung. Second, in the experimental system the rod-roughness was depressed to below the smooth wall, whereas in the DNS the rods protruded from the smooth wall.

Fig. 3 shows the distribution of turbulent Reynolds shear stress over a spatially developing turbulent boundary layer with a rod-roughened wall. These velocity fields were generated by combining six velocity fields recorded at various positions along the downstream direction. The streamwise distance from the step change region is normalized by the boundary layer thickness at the first rod. Turbulent Reynolds shear stress are normalized by the friction velocity in the downstream region ($x/\delta_0 = 5.4$). Fig. 3 shows that the turbulent Reynolds shear stress increases near the step change region, and that a rough wall turbulent boundary layer gradually grows as the flow moves downstream. A self-preservation of the rough wall TBL is shown in Figs. 4 and 5 by comparing the profiles of streamwise mean velocity at four downstream locations. The mean velocity is normalized by the local friction velocity at each position. As shown in Fig. 4a, a new logarithmic layer is developed after the step change of the surface roughness and the deviation of the streamwise mean velocity in the logarithmic layer between smooth and rough walls is $\Delta U^+ = 8.1$. The corresponding effective sand roughness height is $k_s^+ = 102.8$, which is sufficiently large for developing a fully rough TBL. The velocity-defect forms of the streamwise mean velocity shown in Fig. 4b satisfy a self-preservation after $x/\delta_0 > 5.4$ from the step change of the surface roughness. The wall-normal distance is normalized by the height of the virtual origin and the boundary layer thickness as follows: $y' = (y-\varepsilon)/\delta$. There is a deviation of the defect forms between the smooth and rough walls in the region $y'/\delta_0 < 0.5$. This may be due to the strong wake strength in the outer layer for the rough wall, as observed by Krogstad et al. (1992).

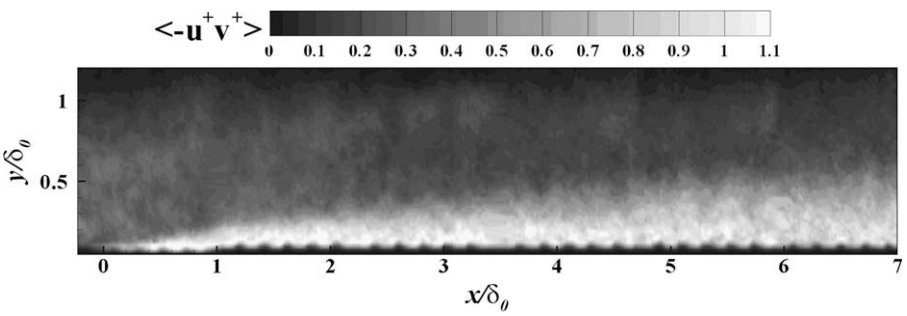

Fig. 3. Iso-contour of turbulent Reynolds shear stress on a rough wall turbulent boundary layer.

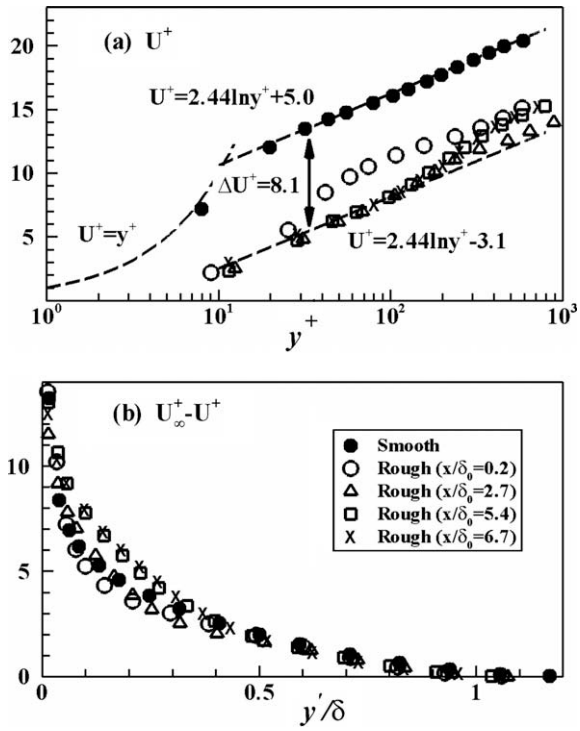

Fig. 4. Variations of streamwise mean velocity along the downstream.

Lee and Sung (2007) used an upstanding rod as the first roughness with $k/\delta_0 = 0.125$ and they observed a self-preservation of turbulent Reynolds stresses after $x/\delta_0 > 30$ from the step change region in their DNS study. Antonia and Luxton (1971) used a depressed rod as the first roughness with $k/\delta_0 = 0.067$ and reported that a self-preservation of turbulent Reynolds stresses is established after $x/\delta_0 > 18$. Fig. 5 shows the profiles of the turbulent Reynolds stress at four downstream locations above the rough wall. After $x/\delta_0 = 5.4$ from the step change region, the turbulent Reynolds stress profiles in the outer layer collapse well, indicating that a self-preserving form for a rough wall TBL is established. In the present study, the distance that is necessary for self-preservation of the turbulent Reynolds stress is estimated to be about $5–6\delta_0$, which is shorter than the distances reported by Lee and Sung (2007) and Antonia and Luxton (1971). As mentioned above, this discrepancy may be due to the use in the present work of a smaller ratio of the roughness height to the boundary layer thickness at the first rod (k/δ_0), as well as the use of a depressed rod at the step change region. Thus, to reduce the effect of the step change in roughness, the first roughness element should be depressed below the smooth wall (Fig. 1) and have a much smaller height than the boundary layer thickness at the step change region.

Fig. 6 shows the comparison of turbulent Reynolds stresses between smooth and rough walls. The lines on Fig. 6 represent the locations of $y = 5k$ (dash-dot) and $y = 5k_s$ (dash). In Fig. 6a, the peak of the turbulent Reynolds stress is smaller for the rough wall than for the smooth wall, owing to the blockage effect of the rod-roughness. In Figs. 6b and c, the wall-normal stress and Reynolds shear stress of the rough wall increase significantly compared to those of the smooth wall. These roughness effects on the turbulent Reynolds stress are observed below $y'/\delta = 0.5–0.6$, which corresponds

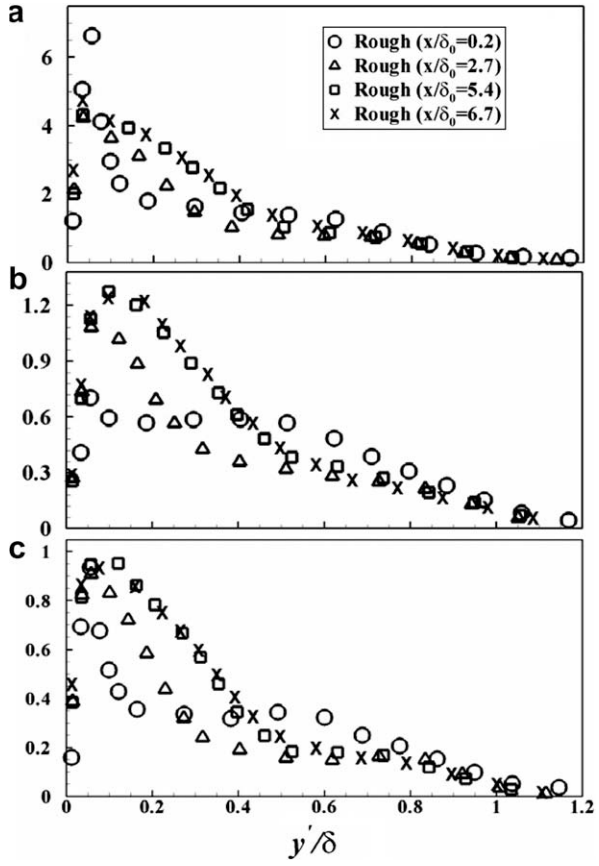

Fig. 5. Variations of the turbulent Reynolds stresses along the downstream: (a) $\langle u^{+2}\rangle$; (b) $\langle v^{+2}\rangle$; (c) $\langle -u^{+}v^{+}\rangle$.

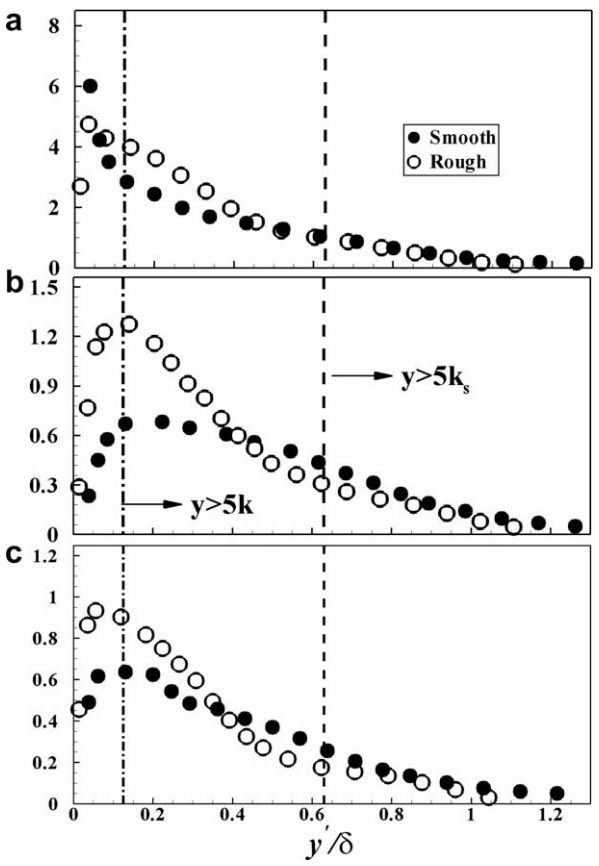

Fig. 6. Comparison of turbulent Reynolds stresses between smooth and rough walls: (a) $\langle u^{+2}\rangle$; (b) $\langle v^{+2}\rangle$; (c) $\langle -u^{+}v^{+}\rangle$.

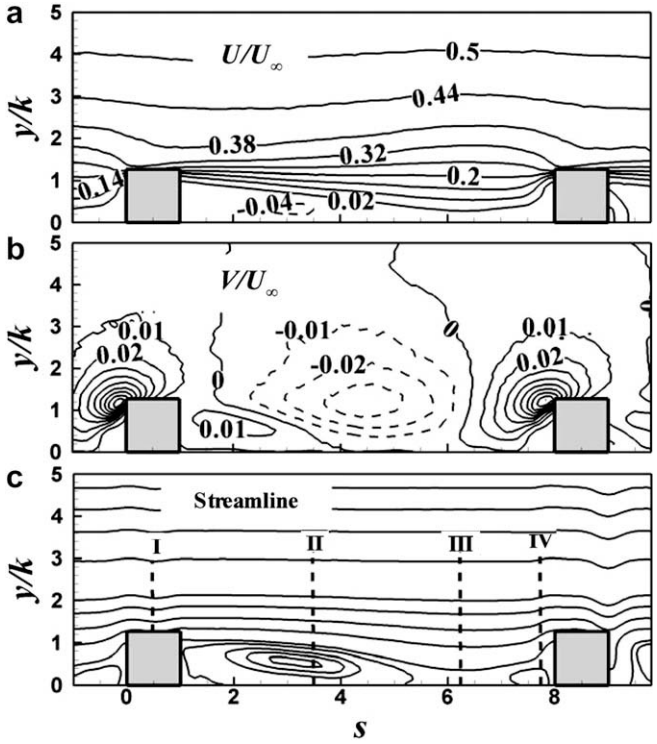

Fig. 7. Iso-contours of mean velocity and streamline in the roughness sublayer. PIV data: (a) U/U_∞; (b) V/U_∞; (c) streamline.

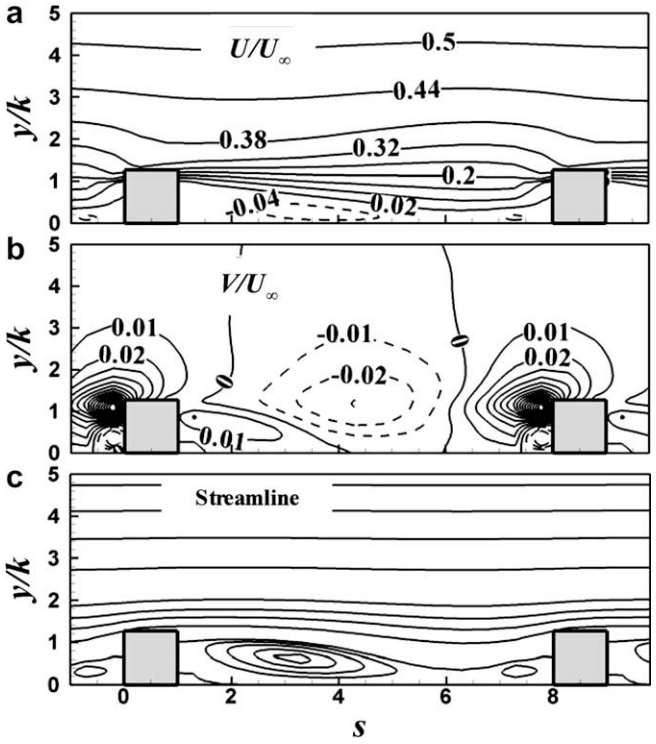

Fig. 8. Iso-contours of the mean velocity and streamline in the roughness sublayer. DNS data: (a) U/U_∞; (b) V/U_∞; (c) streamlines.

to 20–30k. Above the surface layer, the profiles of the turbulent Reynolds stresses of the smooth and rough walls are almost indistinguishable within the experimental uncertainties. Lee and Sung (2007) defined the roughness sublayer as the layer where the turbulent statistics are spatially inhomogeneous; using this definition, they estimated the thickness of the roughness sublayer (ζ) to be about 5k. In the present study, we found that the turbulent statistics became spatially homogeneous above $y = 5k$. Thus, using the definition of ζ proposed by Lee and Sung (2007), we defined the roughness sublayer to be the region of $y < 0.125\delta$ ($=5k$), and the

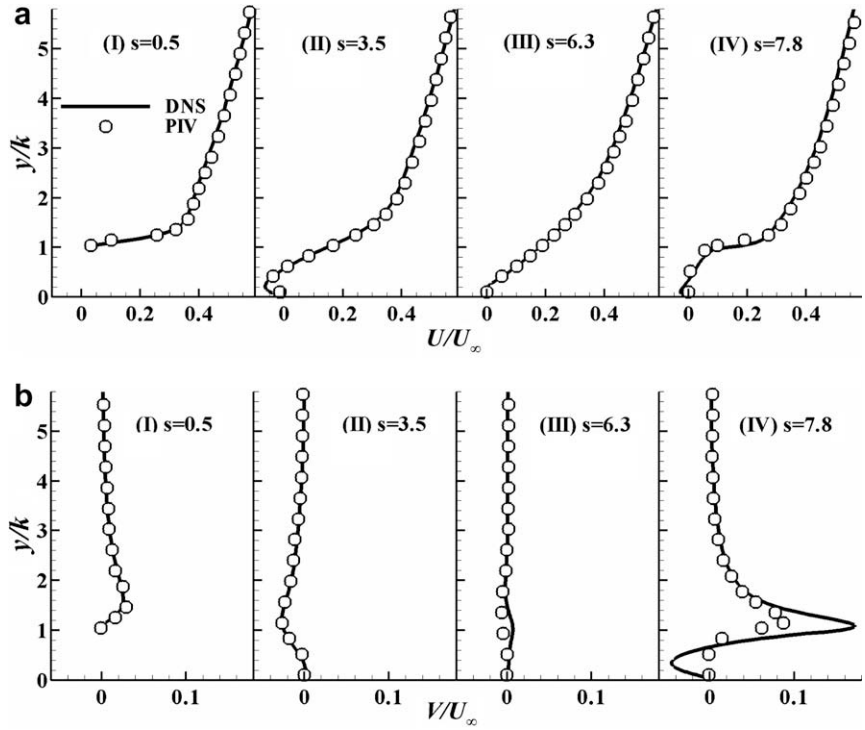

Fig. 9. Comparison of mean velocity by PIV with that of DNS: (a) U/U_∞; (b) V/U_∞.

outer layer to be above the roughness sublayer. This indicates that the effects of rod-roughness on the turbulent Reynolds stress hold not only in the roughness sublayer but also in the outer layer, in agreement with Lee and Sung (2007). Note that the roughness effect on the outer layer can be observed, even though the height of rod-roughness satisfies the criterion of Jimenez (2004), $k/\delta \leqslant 0.025$.

Schultz and Flack (2005) proposed that the effective sand roughness height (k_s) is a better representative length scale than the roughness height (k), and that the extent of the roughness sublayer is $5k_s$ rather than $5k$. In another study examining the critical roughness height for outer layer similarity in flows over sand grain and woven mesh roughness elements, Flack et al. (2007) proposed that the layer directly influenced by the roughness is confined to a region of $y < 3k_s$. When we employ k_s as a representative length scale, the region where the rod-roughness can affect the TBL is confined to $y < 4$–$5k_s$, which is slightly larger than that of Flack et al. (2007).

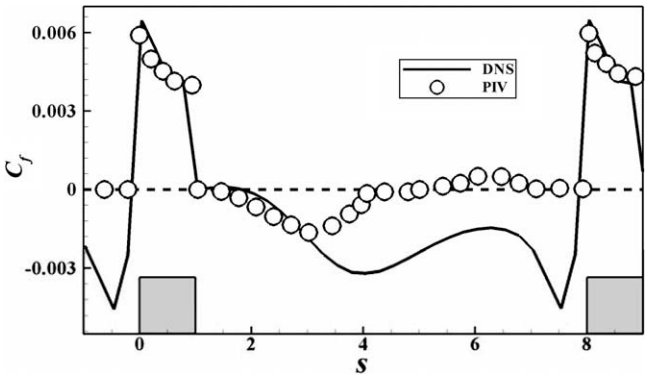

Fig. 10. Streamwise variations of the skin friction coefficient along the rough wall. Dotted line represents the line of $C_f = 0$.

Fig. 7 shows iso-contours of the mean velocity and streamlines in the roughness sublayer obtained from the present PIV measurements, while Fig. 8 shows the corresponding data from the DNS of Lee and Sung (2007). The distance along the streamwise direction normalized by the roughness height (i.e. $s = (x - x_0)/k$) is used, where x_0 is the distance to the reference position (leading edge of the rod located sufficiently downstream the step change region). The wall-normal distance is normalized by the roughness height and the mean velocity is normalized by the free-stream velocity. The iso-contours of the mean velocity and streamlines obtained by PIV are in very good agreement with those of the DNS. In particular, the locations of the vortex core in a cavity, as well as the locations of the local maxima and minima of the wall-normal mean velocity are almost the same in the PIV and DNS data. Fig. 9 compares the mean velocity profiles obtained by PIV at four locations (I)–(IV) marked in Fig. 7c with those of the DNS of Lee and Sung (2007). The mean velocity profiles obtained by PIV collapse very well onto those obtained by DNS when they are normalized by the free-stream velocity and the roughness height. Very near the leading edge of the rod at location (IV), a small deviation is observed in the wall-normal mean velocity below $y < 2k$. Fig. 10 shows the variations of the skin friction coefficient measured by PIV along the rod-roughened wall, along with the profiles obtained by DNS (Lee and Sung, 2007). The skin friction coefficient increases abruptly above the crest of the rod, and decreases to a negative value in the cavity due to the recirculating flow. The sign of the skin friction coefficient changes near $s = 4$ and has a positive value after $s > 4$. This observation seems to suggest that there is a reattachment region near $s = 4$; however, Lee and Sung (2007) and Ashrafian et al. (2004) reported that there is no reattachment region in the cavity for $\lambda = 8k$. In Fig. 10, the skin friction coefficient obtained in the DNS has a negative value along the bottom wall of the cavity except very near the trailing edge ($1 < s < 1.8$). This discrepancy

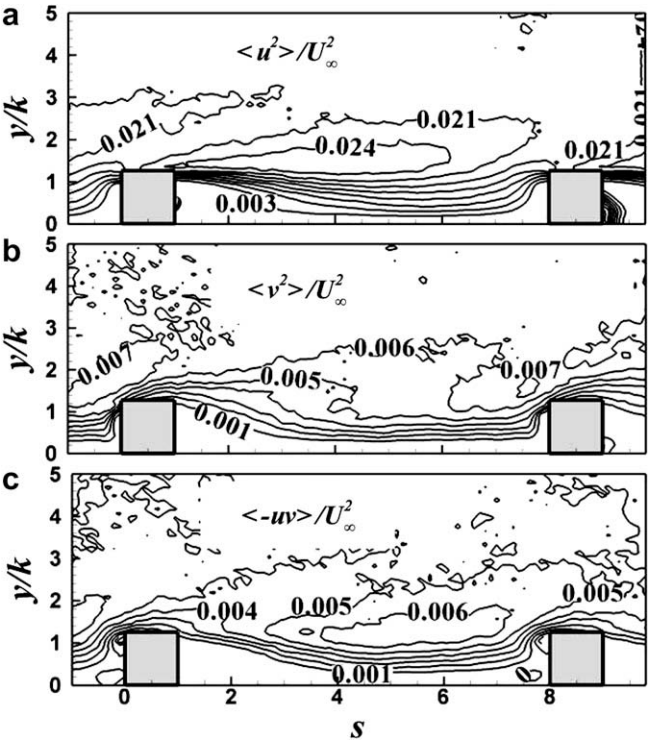

Fig. 11. Iso-contours of turbulent Reynolds stress in the roughness sublayer. PIV data: (a) $<u^2>/U_\infty^2$; (b) $<v^2>/U_\infty^2$; (c) $<-uv>/U_\infty^2$.

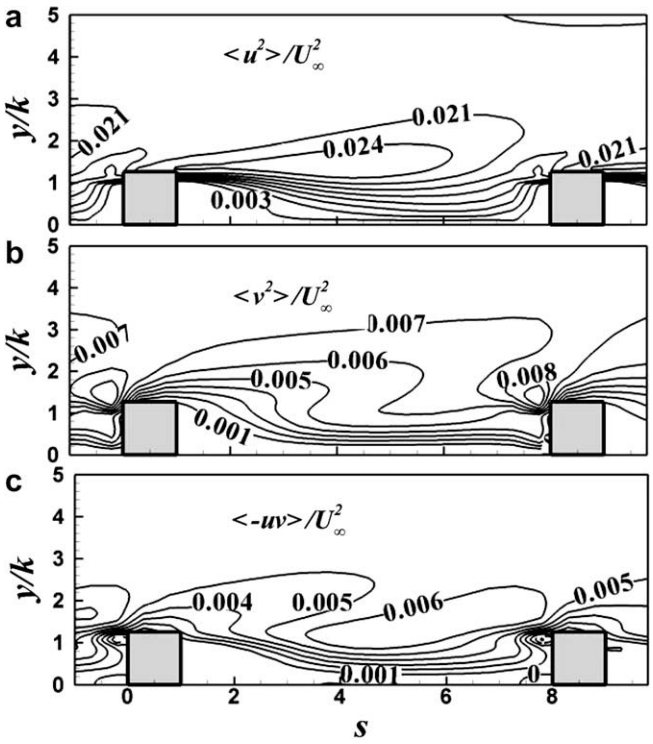

Fig. 12. Iso-contours of turbulent Reynolds stress in the roughness sublayer. DNS data: (a) $<u^2>/U_\infty^2$; (b) $<v^2>/U_\infty^2$; (c) $<-uv>/U_\infty^2$.

between the PIV and DNS findings may be due to the limited spatial resolution of PIV along the wall-normal direction. After the middle of the cavity, there is a very thin layer below $y/k < 0.1$ where the streamwise mean velocity has a negative value. In the present study using PIV, the skin friction coefficient is calculated by using the wall-normal gradient of the streamwise mean velocity with the first two velocity vectors from the wall. The nearest vector from the wall is placed at $y/k \sim 0.1$ and the second vector is placed at $y/k \sim 0.2$. Thus, the negative skin friction coefficient may not be detected after $s > 4$ in the present PIV measurements. This indicates that if the skin friction coefficient over the bottom wall in the cavity is to be accurately measured, the spatial resolution of PIV along the wall-normal direction would need to be increased to $\Delta y/k < 0.05$.

Iso-contours of the turbulent Reynolds stress in the roughness sublayer of the present PIV measurements are shown in Fig. 11, and the corresponding data obtained by DNS (Lee and Sung, 2007) are shown in Fig. 12. In these figures, the turbulent Reynolds stresses are normalized by the free-stream velocity. In front of the leading edge, small regions of negative Reynolds shear stress are observed. The PIV contours are in good agreement with those obtained by DNS. The locations of the maximum streamwise velocity fluctuations and Reynolds shear stress are very similar to those obtained by DNS. However, in the vicinity of the leading edge or the crest of the rod, the wall-normal velocity fluctuations are slightly less intense in the PIV data than in the DNS data. The profiles of the turbulent Reynolds stresses obtained using PIV at the same locations as in Fig. 9 are compared with those obtained by DNS in Fig. 13. Note that the iso-contours of mean velocity and turbulent Reynolds stress obtained by PIV collapse well onto those obtained by DNS, even though the roughness height and flow conditions are different. This indicates that the roughness height and free-stream velocity are more adequate length and velocity scales in the roughness sublayer compared to the viscous length scale and friction velocity. Very near the leading edge of the rod location (IV), there is a discrepancy between the PIV and DNS wall-normal velocity fluctuations below $y < 2k$. This may be caused by errors in the PIV measurements due to the presence of the wall and the strong velocity gradient near the roughness.

Fig. 14 shows the instantaneous velocity fields and vortical structures near the roughness sublayer. Galilean decomposition is applied to the instantaneous velocity vectors with the reference velocity $U_c = 0.7U_\infty$ in Fig. 14a and with the reference velocity $U_c = 0.5U_\infty$ in Fig. 14b (Adrian et al., 2000). Vortical structures,

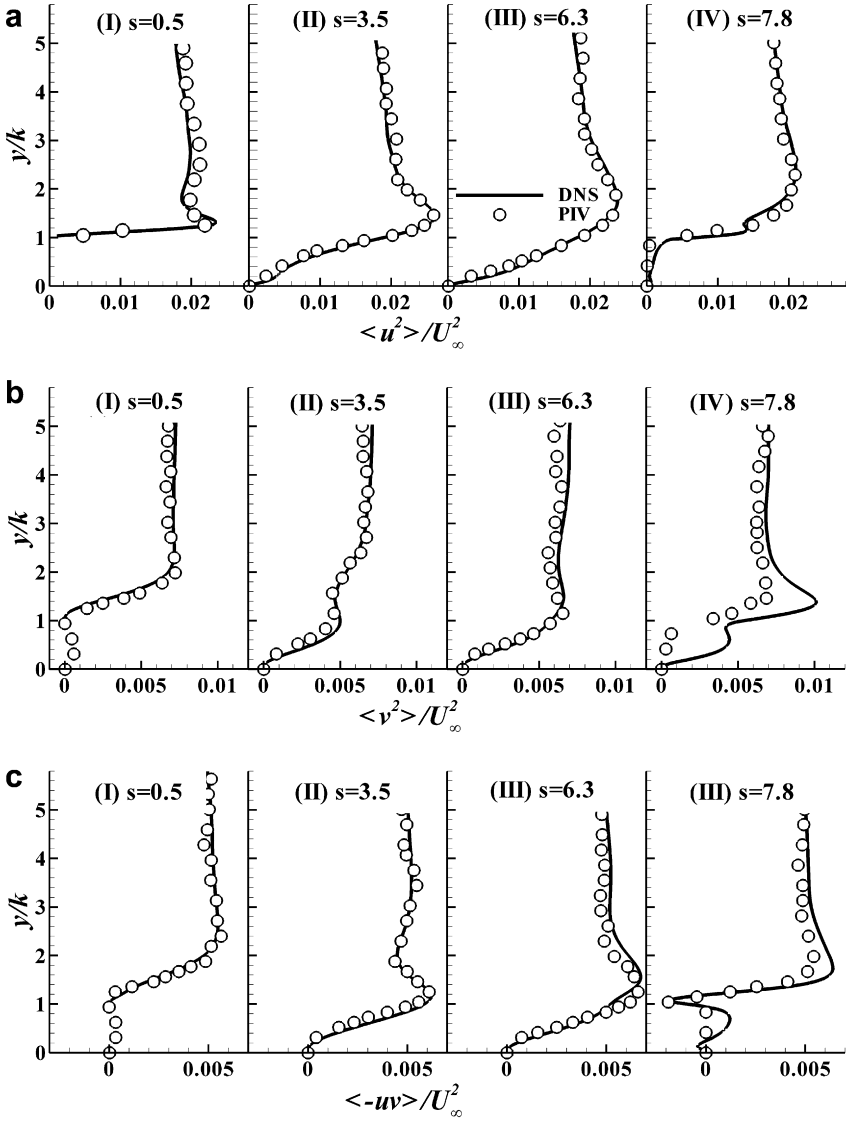

Fig. 13. Comparison of turbulent Reynolds stress by PIV with that of DNS: (a) $\langle u^2\rangle/U_\infty^2$; (b) $\langle v^2\rangle/U_\infty^2$; (c) $\langle -uv\rangle/U_\infty^2$.

identified by a positive value of the swirling strength λ_{ci}, are detected, where λ_{ci} is the imaginary part of the complex conjugate eigenvalues of the local velocity gradient tensors. The conjugate pairs of the complex eigenvalues $\lambda_{cr} \pm \lambda_{ci}i$ are calculated by solving the characteristic equation of the velocity gradient tensor,

$$\det|D - \lambda I| = \begin{vmatrix} \frac{\partial u}{\partial x} - \lambda & \frac{\partial u}{\partial y} \\ \frac{\partial v}{\partial x} & \frac{\partial v}{\partial y} - \lambda \end{vmatrix} = 0,$$

where D is the velocity gradient tensor (Zhou et al., 1999). The swirling strength is frame-independent and discriminates compact vortical cores from regions of intense shear. Two vortices at $y = 5$–$6k$ with reference velocity $U_c = 0.7U_\infty$ are observed in Fig. 14a, and two vortices near the crest of the rod with reference velocity $U_c = 0.5U_\infty$ are observed in Fig. 14b. These vortices have sizes on the order of the rod height and are inclined at approximately 33° with respect to the downstream direction. The two upper vortices are moving with higher convection velocities, whereas the lower vortices are moving with lower convection velocity. The lower vortices resemble those reported by Wang et al. (2007), who observed several vortices shedding from the rod in the region of $1 < y/k < 3$, all with the same convection velocity ($U_c = 0.52U_\infty$) and an angle of inclination of 20°. In the middle of the cavity ($s = 3$–5), a region of very large swirling strength is observed; this may be related with the downward sweep motion and shedding vortices induced from the rod. Fig. 14c shows vector fields of instantaneous velocity fluctuations, where high speed fluid rushes in toward the cavity region. This sweep event occurs strongly above and inside the cavity.

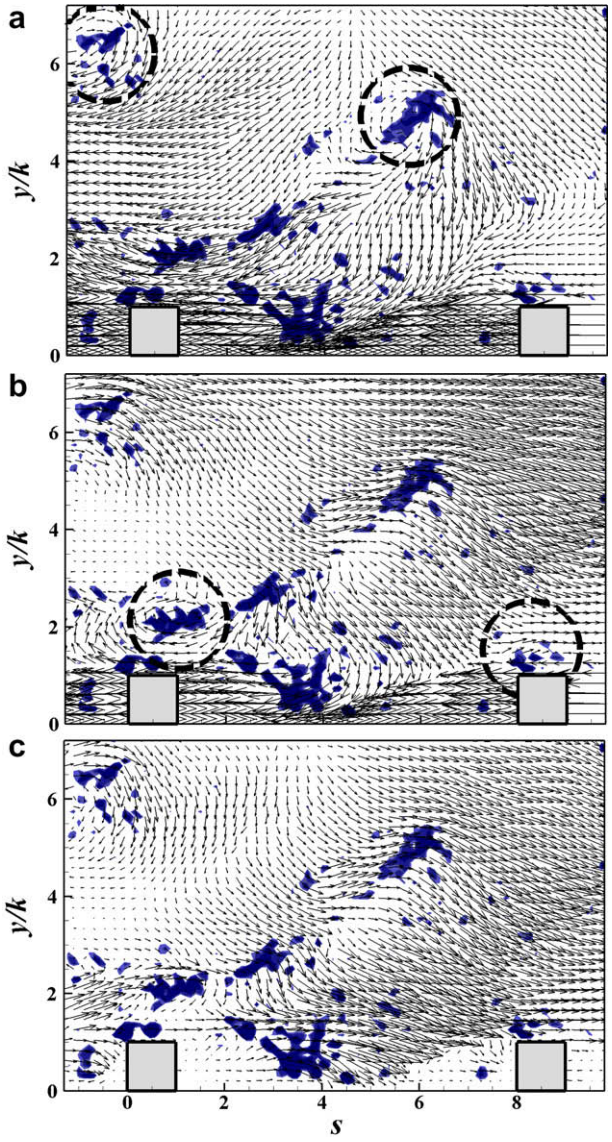

Fig. 14. Visualizations of vortical structures near the roughness sublayer. Isocontour represents the swirling strength. Vortices are emphasized by dotted circles: (a) instantaneous velocity vector field with the reference frame velocity $U_f = 0.7U_\infty$; (b) instantaneous velocity vector field with the reference frame velocity $U_f = 0.5U_\infty$; (c) instantaneous vector field of velocity fluctuations (u', v').

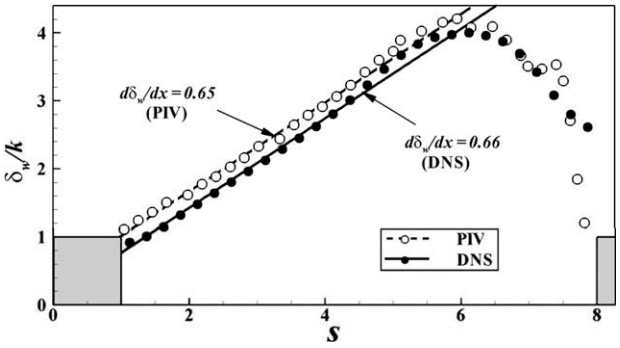

Fig. 15. Streamwise variation of the vorticity thickness along the rough wall. Dotted and solid lines represent linear fitted lines in the region of $1 < s < 6$.

In Fig. 14, several vortices can be discerned that seem to be separated from the rod-roughness. To quantify the growth rate of the shear layer, the vorticity thickness δ_w is calculated as follows:

$$\delta_w = \frac{U_1 - U_2}{(dU/dy)_{max}},$$

where $(dU/dy)_{max}$ is the maximum velocity gradient in the shear layer, and U_1 and U_2 are the speeds of the upper and lower streams in the mixing layer, respectively (Brown and Roshko, 1974). In the present study, we used U_1 as the free-stream velocity U_∞ and $U_2 = 0$. In Fig. 15, the vorticity thickness obtained using PIV is compared with that obtained by DNS. Despite of small discrepancy of the vorticity thickness, the growth rate of the shear layer is almost the same between PIV and DNS. As shown in Fig. 15, the growth rate of the shear layer is almost linear in the region $1 < s < 6$, indicating that the shear layer separated from the rod is developing in this region with a growth rate of $d\delta_w/dx = 0.65$–0.66. This growth rate is higher than the value of 0.21 obtained by Wang et al. (2007) for a channel flow with a two-dimensional rod-roughened wall ($k/h = 0.15$, h is channel height) and that of 0.18 obtained by Brown and Roshko (1974) for a plane mixing layer. This difference may be due to the different flow configurations (plane mixing layer or wall-bounded flow) or different roughness geometries (k/δ or λ/k). This also might be due to use of the free-stream velocity for U_1, which is too large to be a velocity scale near the rod-roughness because the roughness height is very small compared to the boundary layer thickness. If we employ the streamwise mean velocity at $y/k = 1.3$ above the crest of the rod, where the shear rate of the streamwise mean velocity decreases significantly, as U_1 rather than the free-stream velocity, $d\delta_w/dx$ has a value of 0.184, which agrees well with the previous results of Brown and Roshko (1974) for a plane mixing layer.

4. Conclusions

PIV measurements of TBLs over smooth and rod-roughened walls were carried out to elucidate the effects of surface roughness on a TBL. The roughness elements employed were periodically ar-

ranged two-dimensional spanwise rods, and the roughness height was $k/\delta = 0.025$, which satisfies the criterion of Jimenez (2004). The spatially developing characteristics of the rough wall TBL were examined and self-preserving forms of the streamwise mean velocity and the turbulent Reynolds stress tensors were obtained with moving downstream over the smooth and rough walls. The distance that is necessary for self-preservation of turbulent Reynolds stresses was estimated to be about $5–6\delta_0$, which is smaller than those obtained by Lee and Sung (2007) and Antonia and Luxton (1971). This discrepancy may be related to the smaller ratio of roughness height to boundary layer thickness at the first rod (k/δ_0) and the use of a depressed rod in the step change region. Introduction of the roughness elements augmented the wake strength in the outer layer. The turbulent Reynolds stresses were also affected below $y'/\delta = 0.5–0.6$, which corresponds to $20–30k$, indicating that the roughness effects are not confined to the roughness sublayer when the thickness of the roughness sublayer was defined as $\zeta = 5k$. This is in agreement with the DNS results of Lee and Sung (2007), even though the height of the rod-roughness in the present study was half that used in the DNS and satisfied the criterion of Jimenez (2004), $k/\delta \leqslant 0.025$. If we employed the effective sand roughness height (k_s) as a representative length scale rather than the roughness height (k), the extent of roughness effect was confined below $y = 4–5k_s$. This supported the assertions of Schultz and Flack (2005) and Flack et al. (2007). The iso-contours of mean velocity and turbulent Reynolds stress in the roughness sublayer obtained by PIV showed very good agreements with the DNS of Lee and Sung (2007) except near the leading edge or the crest of the rod. In the roughness sublayer, we observed the separated shear layer and vortical structure induced by the two-dimensional rod-roughness. In the middle of the cavity, a region of very large swirling strength was observed, providing strong evidence of vortices induced by shedding from the rod which might be related to the downward sweep motion. The sweep event occurs strongly above and inside the cavity.

Acknowledgement

This work was supported by the Basic Research Program (R01-2004-000-10521-0) and Acceleration Research (R17-2007-055-01000-0) of the Korea Science and Engineering Foundation, and partially by the support from KISTI Supercomputing Center (KSC-2007-S00-1017).

References

Adrian, R.J., Christense, K.T., Liu, Z.-C., 2000. Analysis and interpretation of instantaneous turbulent velocity fields. Exp. Fluids 29, 275–290.

Antonia, R.A., Luxton, R.E., 1971. The response of a turbulent boundary layer to a step change in surface roughness Part 1. Smooth to rough. J. Fluid Mech. 48, 721–761.

Ashrafian, A., Andersson, H.I., Manhart, M., 2004. DNS of turbulent flow in a rod-roughened channel. Int. J. Heat Fluid Flow 25, 373–383.

Bakken, O.M., Krogstad, P.-Å., 2005. Reynolds number effects in the outer layer of the turbulent flow in a channel with rough walls. Phys. Fluids 17, Article #065101.

Bhaganagar, K., Kim, J., Coleman, G., 2004. Effect of roughness on wall-bounded turbulence. Flow Turbul. Combust. 72, 463–492.

Brown, G.L., Roshko, A., 1974. On density effects and large structure in turbulent mixing layer. J. Fluid Mech. 64, 775–816.

Djenidi, L., Antonia, R.A., Amielh, M., Anselmet, F., 2008. A turbulent boundary layer over a two-dimensional rough wall. Exp. Fluids 44, 37–47.

Flack, K.A., Schultz, M.P., Shapiro, T.A., 2005. Experimental support for Townsend's Reynolds number similarity. Phys. Fluids 17, Article #035102.

Flack, K.A., Schultz, M.P., Connelly, J.S., 2007. Examination of a critical roughness height for outer layer similarity. Phys. Fluids 19, Article #095104.

Hart, D.P., 2000. PIV error correction. Exp. Fluids 29, 13–22.

Islam, M.S., Haga, K., Kaminaga, M., Hino, R., Monde, M., 2002. Experimental analysis of turbulent flow structure in a fully developed rib-roughened rectangular channel with PIV. Exp. Fluids 33, 296–306.

Jimenez, J., 2004. Turbulent flows over rough walls. Annu. Rev. Fluid Mech. 36, 173–196.

Keirsbulck, L., Labraga, L., Mazouz, A., Tournier, C., 2002. Surface roughness effects on turbulent boundary layer structures. J. Fluids Eng. 124, 127–135.

Krogstad, P.-Å., Antonia, R.A., 1999. Surface roughness effects in turbulent boundary layers. Exp. Fluids 27, 450–460.

Krogstad, P.-Å., Antonia, R.A., Browne, L.W.B., 1992. Comparison between rough- and smooth-wall turbulent boundary layers. J. Fluid Mech. 245, 599–617.

Krogstad, P.-Å., Andersson, H.I., Bakken, O.M., Ashrafian, A., 2005. An experimental and numerical study of channel flow with rough walls. J. Fluid Mech. 530, 327–352.

Lee, C.H., 2002. Large-eddy simulation of rough-wall turbulent boundary layer. AIAA J. 40, 2127–2130.

Lee, S.-H., Sung, H.J., 2007. Direct numerical simulation of turbulent boundary layer over a rod-roughened wall. J. Fluid Mech. 584, 125–146.

Leonardi, S., Orlandi, P., Smalley, R.J., Djenidi, L., Antonia, R.A., 2003. Direct numerical simulations of turbulent channel flow with transverse square bars on one wall. J. Fluid Mech. 491, 229–238.

Morris, S.C., Stolpa, S.R., Slaboch, P.E., Klewicki, J.C., 2007. Near-surface particle image velocimetry measurements in a transitionally rough-wall atmospheric boundary layer. J. Fluid Mech. 580, 319–338.

Nitche, W., Thunker, R., Haberland, C., 1983. A computational preston tube method. In: Proceedings of the Fourth Symposium on the Turbulent Shear Flows, pp. 261–276.

Pokrajac, D., Campbell, L.J., Nikora, V., Manes, C., McEwan, I., 2007. Quadrant analysis of persistent spatial velocity perturbations over square-bar roughness. Exp. Fluids 42, 413–423.

Raupach, M.R., Antonia, R.A., Rajagopalan, S., 1991. Rough-wall turbulent boundary layers. Appl. Mech. Rev. 44, 1–25.

Scarano, F., Riethmuller, M.L., 1999. Iterative multigrid approach in PIV image processing with discrete window offset. Exp. Fluids 26, 513–523.

Schultz, M.P., Flack, K.A., 2005. Outer layer similarity in fully rough turbulent boundary layers. Exp. Fluids 38, 328–340.

Schultz, M.P., Flack, K.A., 2007. The rough-wall turbulent boundary layer from the hydraulically smooth to the fully rough regime. J. Fluid Mech. 580, 381–405.

Townsend, A.A., 1976. The Structure of Turbulent Shear Flow. Cambridge University Press, Cambridge.

Volino, R.J., Schultz, M.P., Flack, K.A., 2007. Turbulence structure in rough- and smooth-wall boundary layers. J. Fluid Mech. 592, 263–293.

Wang, L., Hejcik, J., Sunden, B., 2007. PIV measurement of separated flow in a square channel with streamwise periodic ribs on one wall. J. Fluid Eng. 129, 834–841.

Westerweel, J., 1994. Efficient detection of spurious vectors in particle image velocimetry data. Exp. Fluids 16, 236–247.

Zhou, J., Adrian, R.J., Balachandar, S., Kendall, T.M., 1999. Mechanism for generating coherent packets of hairpin vortices. J. Fluid Mech. 387, 353–396.